Chinese Chemical Letters 35 (2024) 108747

Contents lists available at ScienceDirect

Chinese Chemical Letters

journal homepage: www.elsevier.com/locate/cclet

Mechanism of nanoparticle aggregation in gas-liquid microfluidic mixing

Hongxia Li[a,*], Xiyang Wang[a], Du Qiao[a], Jiahao Li[a], Weiping Zhu[b], Honglin Li[b]

[a] Key Laboratory for Precision & Non-traditional Machining Technology of Ministry of Education, Dalian University of Technology, Dalian 116023, China
[b] Shanghai Key Laboratory of New Drug Design, School of Pharmacy, East China University of Science and Technology, Shanghai 200237, China

ARTICLE INFO

Article history:
Received 19 April 2023
Revised 16 June 2023
Accepted 27 June 2023
Available online 2 July 2023

Keywords:
Microfluidic
Gas-liquid segmented micromixer
Nanoparticle aggregation
Shear effect
Numerical calculation

ABSTRACT

Using gas-liquid segmented micromixers to prepare nanoparticles that have a homogeneous particle size, controllable shape, and monodispersity advantages. Although nanoparticle aggregation within a microfluid has been shown to be affected by the shear effect, the shear effect triggering conditions in gas-liquid two-phase flow is unclear and the aggregation behavior of nanoparticles under the shear effect is difficult to predict, resulting in uncontrollable physical and chemical properties of nanoparticle aggregates. In this study, a numerical simulation of nanoparticle aggregation in gas-liquid two-phase flow under the shear effect is performed using the CFD-DEM method. Then, the effects of total flow rate, gas-liquid two-phase flow ratio, and particle volume fraction on particle aggregation were analyzed to achieve control of particle aggregation shape and size. Meanwhile, the triggering mechanism of the shear effect and the mechanism of the shear effect on the aggregation of nanoparticles were clarified. The results show that increasing the total flow rate or decreasing the gas-liquid two-phase flow rate ratio can induce the shear effect, which reduces the particle aggregation size and makes the morphology tend to be spherical. Moreover, increasing the particle volume fraction, and total flow rate or decreasing the gas-liquid two-phase flow rate ratio also increases the number of particle collisions and induce interparticle adhesion. Hence, particle adhesion and the shear effect compete with each other and together affect particle aggregation.

Nanoparticle drug delivery systems show great potential for cancer therapy and targeted disease treatment [1,2]. Furthermore, for better drug loading capacity and stability, the nanoparticle drug delivery system should be as small as possible and have uniform morphology and homogeneous size [3–5]. However, using the bulk preparation method to prepare nanoparticle drug delivery systems is associated with slow mixing speed and uncontrolled flow field, which leads to the wide size distribution of nanoparticles, inhomogeneous morphology, and poor batch-to-batch reproducibility. While the micro-mixing chip has shown good promise in the preparation of nanoparticle drug delivery systems because of its high mixing efficiency and precise fluid control [6].

Segmented flow micromixers (SMFRs) in micro-mixing chips produce slug flow (gas-liquid segmented micromixer)/droplet flow (liquid-liquid segmented micromixer) by adding gas or liquid incompatible with solvents. The reverse circulation generated in droplets and recirculation in slug enhances the solvent mixing rate and radial solute transport, resulting in the reduction of nanoparticle aggregate size and the enhancement of monodispersity. Stolzenburg *et al.* [7] prepared TiO_2, ZnO, and CeO_2 nanoparticles using liquid-liquid segmented micromixers and adapted to different reaction times by changing the microchannel structure. Moreover, Ochoa *et al.* [8] proposed a simple and low-cost liquid-liquid segmented flow method for the synthesis of spherical nanoparticles of Ag and Au and reduced the particle size by varying the reactant concentration, reaction time, temperature and surface tension. While Kumar *et al.* [9] used both gas-liquid segmented micromixer and liquid-liquid segmented micromixer to prepare Ag nanoparticles. Under the same operating conditions, due to different hydrodynamic effects, the gas-liquid two-phase micromixer generated particle aggregates with better morphology, smaller particle size and narrower size distribution. In addition, the gas-liquid segmented micromixer is more widely used because the gas phase can be separated more easily. Therefore, many researchers used the gas-liquid segmented micromixer to prepare nanoparticles. For example, Huang *et al.* [10] prepared Au nanoparticles using gas-liquid segmented micromixer and accelerated the mixing rate by opti-

* Corresponding author.
E-mail address: hxli@dlut.edu.cn (H. Li).

https://doi.org/10.1016/j.cclet.2023.108747
1001-8417/

mizing the flow conditions to achieve nanoparticles polydispersity of less than 5%. Kwak *et al.* [11] used gas-liquid segmented micromixer to synthesize CdSe quantum dots and uniform nanoparticles size distribution by adjusting the precursor flow rate. It is seen that changing the total flow rate, two-phase flow rate can improve the mixing rate and thus control the morphology and size of the particle aggregates. However, Wang *et al.* [12–14] found the shear effect within the gas-liquid segmented micromixer in their experiments and showed that the morphology and size of the particle aggregates were also affected by it.

When the particle aggregates are in the fluid domain with velocity gradient, the magnitude and direction of the hydrodynamic forces on both sides are different, producing the shear effect and inducing particle aggregates to separate. To clarify the influence of the shear effect on the aggregation behavior and dynamics of nanoparticles, researchers obtained the collision frequency and force between particles by constructing numerical simulations. For example, Becker *et al.* [15–17] constructed a computational model based on experimental data that can accurately describe the interparticle interaction forces and used it to investigate the reorganization behavior of particle aggregates within a linear shear flow in relation to the size of the aggregates. Moreover, Wilson *et al.* [18–20] analyzed the factors influencing the size and monodispersity of particle aggregates within the Poisson leaf flow in microchannels and showed that the size of aggregates increases and then decreases with increasing flow velocity and shows polydispersity. Furthermore, Zeidan *et al.* [21,22] clarified the fracture mechanism of aggregates and showed that the final aggregate morphology is strongly correlated with the shear rate and interparticle interactions. Nanoparticle aggregation behavior in microfluidic channels is strongly influenced by the flow pattern, whereas little attention has been paid to nanoparticle aggregation behavior in gas-liquid two-phase flows. Previous experiments have mostly focused on the analysis of the morphology and monodispersity of nanoparticle aggregates in gas-liquid two-phase flows [23–25], and there are few studies on the effect of flow properties on shear effects and the prediction of nanoparticle aggregation behavior under the shear effect. Therefore, it is not possible to precisely control the morphology and size of nanoparticle aggregates by changing the flow properties.

In this study, a model of nanoparticle aggregation in gas-liquid two-phase flow based on the CFD-DEM method was developed to investigate the effect of the shear effect on nanoparticle aggregation behavior. The van der Waals and adhesion forces between nanoparticles, and the drag force and shear lift forces of the flow field on nanoparticles are considered in this model. We have focused on the effects of total flow velocity, gas-liquid two-phase flow ratio, and particle concentration on particle collision frequency and the shear effect. Furthermore, the trigger conditions of shear effect in gas-liquid two-phase flow are clarified, and the prediction of nanoparticle aggregation behavior within the gas-liquid two-phase flow is realized.

A gas-liquid segmented micromixer structure with Taylor flow pattern in the microchannel was constructed to study the influence of the shear effect on the aggregation of nanoparticles. The structure is schematically shown in Fig. 1, where a slug and two adjacent half bubbles are called a “unit cell”. Since the particle aggregation is only influenced by the flow field inside the slug, the bubble is considered as “void”. The cross-section of the microchannel is circular, and the inner diameter d is 40 μm. L_B and L_S denote the length of bubble and slug, and δ is the thickness of the liquid film, which are related to the physical characteristics of the gas-liquid phase, flow characteristics and microchannel inlet type. In this paper, the microchannel inlet is set as a classical T-shaped inlet with the same inlet characteristic length as the microchannel. L_B, L_S and δ change when the total flow rate of the gas-liquid phase and the two-phase flow rate ratio change. Qian *et al.* [26] and Aussillous *et al.* [27] summarized empirical formulas for L_B, L_S, and δ when the microchannel entrance is T-shaped from experimental data in Eqs. S1-S3 (Supporting information).

At the microscale, the motion of nanoparticles is subjected to buoyancy, drag force, shear lift force (the hydrodynamic force), van der Waals force, and interparticle contact force (the particle interaction force). Since the density of the particles is similar to that of the fluid, gravity and buoyancy are neglected in this study, and the physical and chemical parameters of the nanoparticles are shown in Table S1 (Supporting information). When the particle velocity is different from the fluid velocity, the particle is subject to drag force, and the direction of the drag force is opposite to the direction of the particle relative to the fluid velocity. Moreover, the shear lift force is generally divided into the Magnus force and the Saffman lift force [28]. Due to the relatively high viscosity of the liquid, the Magnus lift force is neglected. When there is a velocity gradient perpendicular to the direction of particle motion in the flow field, the Saffman lift force is directed from the low flow direction to the high flow direction, pushing the particles toward the high flow region. At the macroscale, the classical Hertz-Mindlin contact model [29] can simulate the interparticle contact process and calculate the interparticle collision force. However, at the microscale, the interparticle adhesion and the interparticle van der Waals forces cannot be neglected. The JKR model [30] can describe the interparticle intrinsic relationship through the particle surface energy and elastic energy, and can accurately predict the interparticle adhesion behavior. Oleh *et al.* [31] introduced interparticle adhesion forces and van der Waals forces based on the JKR contact model theory and modified the classical Hertz-Mindlin formulation, and the interparticle contact forces are shown in Eq. S6 (Supporting information).

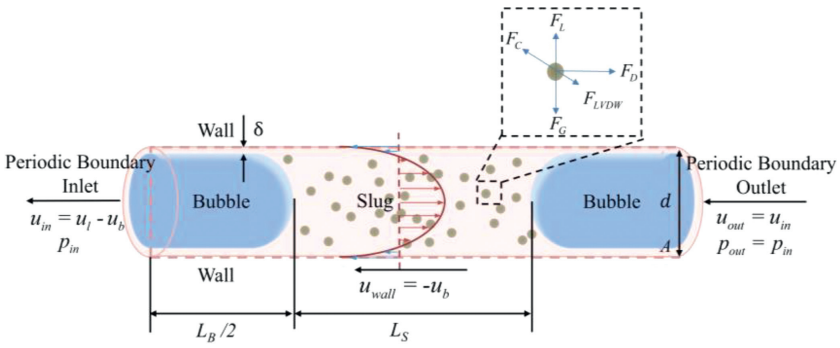

Fig. 1. Schematic structure of nanoparticle aggregation model within gas-liquid two-phase flow. Where u_b is the apparent bubble velocity, and u_l is the liquid phase velocity. The gas-liquid two-phase flow flows from left to right. Due to the use of dynamic reference coordinate system, the periodic boundary velocity is negative, and the direction is opposite to the actual flow direction.

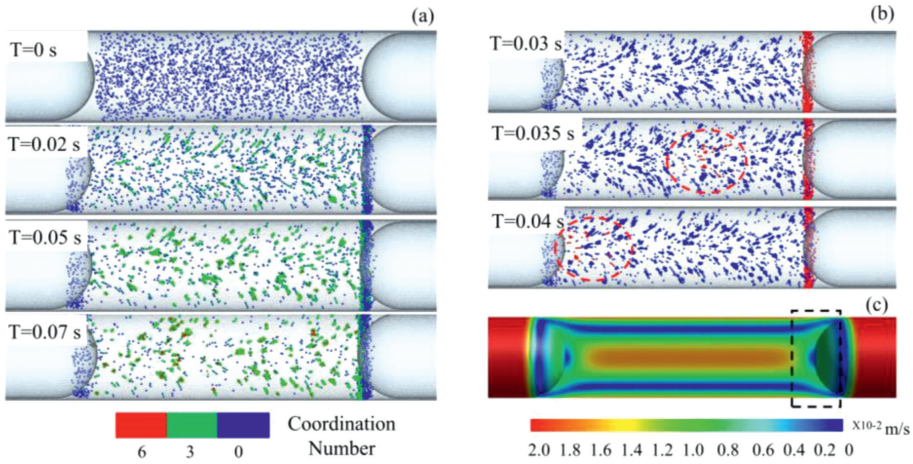

Fig. 2. (a) Particle aggregation in the gas-liquid two-phase flow when the total flow rate $Q = 0.025$ μL/s and the two-phase flow rate ratio is 1:1. (b) The location of the marked particles at $T = 0.03$ s, 0.035 s, 0.04 s. (c) The velocity cloud of the gas-liquid two-phase flow.

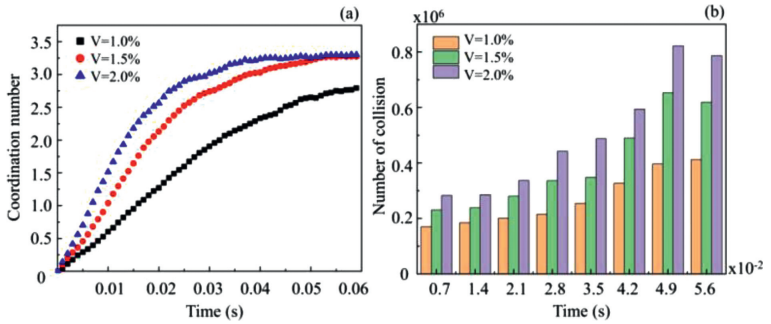

Fig. 3. Variation of average particle coordination number and collision number for a total flow rate of 0.025 μL/s, a two-phase flow rate ratio of 1:1, and particle volume fractions of 1%, 1.5%, and 2%.

In order to simulate the particle aggregation in gas-liquid two-phase flow, the flow field data in the steady state of gas-liquid two-phase flow are first solved, and then the particle motion under the action of the flow field is solved. When the particle concentration is less than 4%, the effect of particle motion on the flow field is negligible [32]. In order to save computational and time costs, the flow field is coupled with the particles in a single term.

When the distance between the centers of two particles is less than the sum of particle radius, the two particles are considered to undergo adhesion. The total number of particles with which a particle adheres is the particle coordination number (C_d). Fig. 2a shows the process of nanoparticles within the liquid slug from a uniformly distributed state to the formation of stable aggregates. The particles are subjected to hydrodynamic forces to start the circular motion. Furthermore, the velocity gradient within the slug causes the particles at different locations to be subjected to different hydrodynamic magnitudes and directions, leading to collisions and adhesion between the particles. And with the increase of time, the particles with high C_d gradually increase and form aggregates.

In addition, deposition was also observed around downstream bubbles, the same deposition observed in the preparation experiments of Au nanostructure by Kulkarni *et al.* [33]. Importantly, severe deposition can affect the stability of gas-liquid two-phase flow and cause preparation contamination, so there is a need to clarify the formation mechanism of deposition and reduce the deposition phenomenon. The deposited particles at $T = 0.03$ s were marked in red and the motion of the marked particles was recorded as shown in Fig. 2b. It is observed that the particles at the deposition will return to the circulation area again after a certain period of time. Comparing the deposition location with the velocity distribution cloud of the flow field (Fig. 2c), it is found that the flow velocity is higher where the particles are deposited compared to other locations. Therefore, the particles are pushed by Saffman lift into the high flow velocity region and form deposition. Then, under the action of drag force, some of the particles at the deposition will restart their circular motion after a short period of parking. In addition, the particles are not stationary during deposition, and there are still collisions between particles. Particle adhesion also occurs at the deposition site and particle aggregates are generated. It is worth noting that a larger drag force is required to restart the cyclic motion of the particle aggregates compared to the particles. Hence, the deposition of particle aggregates may be irreversible when the flow velocity within the flow field is small or the velocity gradient around the bubble is too large.

The variation of C_d and collision number for different particle volume fractions is shown in Fig. 3, where C_d increases with time and tends to a constant value after a certain time (Fig. 3a). The increase in particle volume fraction increases the collision chance between particles and thus increases collision number (Fig. 3b). When the particle volume fraction becomes larger, the increase of collision number makes the adhesion between particles easier, so the stable value of C_d also tends to increase. Therefore, when the number of collisions increases, the particle aggregates become larger. However, when the particle volume fraction changed from 1.5% to 2%, the C_d only increased by 0.85% and the growth trend became smaller. This is because the adhesion capacity of the particles is limited by the surface energy of the particles, and the particle aggregates stop growing when the particles reach the adhesion limit. As we all know, nanoparticles have large specific surface area and surface energy and are in a state of energy instability. Therefore, particles always tend to aggregate with each other, making the aggregate particle size larger, reducing the surface energy and

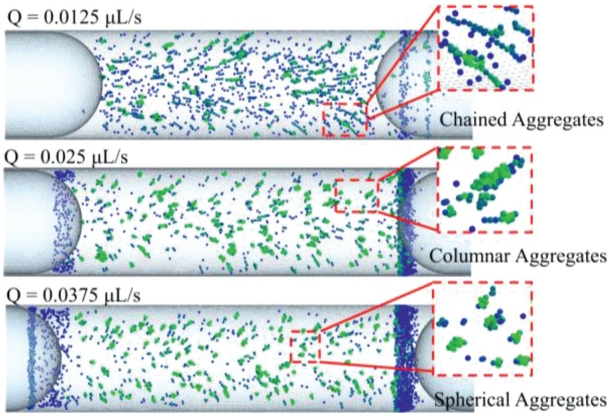

Fig. 4. Changes of particle aggregation morphology at the total flow rate of 0.0125 μL/s, 0.025 μL/s and 0.0375 μL/s with the two-phase flow rate ratio of 1:1, and particle volume fractions of 1%.

making the energy stable [34]. When the energy is stabilized, it is difficult to produce adhesion behavior even if the particles collide with each other again. Hence, when the particle volume fraction is small, the aggregate size is dominated by the collision number. However, at larger particle volume fractions, the particle adhesion ability determines the final aggregate size.

The increase in the total flow rate intensifies the circulation within the slug and the velocity gradient becomes larger. Fig. 4 shows the changes in morphology and size of nanoparticles at different total flow rates. When the total flow rate gradually increases, the nanoparticle aggregates change from chained aggregates to columnar aggregates and finally tend to be spherical aggregates. Figs. 5a and b show the variation of C_d and collision number for different total flow rates. The increase in the total flow rate intensifies the recirculation in the flow field and increases the collisions between the particles. Furthermore, the increase in the number of collisions induces adhesion between particles and larger aggregate size, which is verified in the two sets of simulations at 0.0125 μL/s and 0.025 μL/s. However, the final stable C_d becomes smaller in the simulation with the total flow rate of 0.0375 μL/s. Before 0.02 s, the C_d increases rapidly as the inter-particle collisions become more frequent. But, after 0.02 s the C_d in the total flow rate of 0.0375 μL/s is gradually smaller than that in the total flow rate of 0.025 μL/s. As shown in Figs. 5c and d, increasing the total flow rate also produces a larger velocity gradient, which leads to an increase in the drag force (tangential force Fτ) and shear lift (normal force Fn) on the particles. The velocity gradient in the flow field causes unequal forces on both sides of the particle aggregates and generates the shear force. Moreover, as the nanoparticle aggregates gradually become larger, the shear force also becomes larger. When the shear force is greater than the adhesion force between the two particles, the shear effect occurs, and the aggregates will be sheared. It explains why the C_d in the total flow rate of 0.0375 μL/s is smaller after 0.02 s than in the total flow rate of 0.025 μL/s. Therefore, the final stable C_d decreases under shear even though the total flow rate becomes larger with an increase in the number of collisions. When the total flow rate is small, there is no shear effect, and the particle aggregate size is dominated by interparticle adhesion. Whereas, when the total flow rate is larger, the shear effect is generated. The interparticle adhesion and the shear effect compete with each other and together affect the particle aggregate size. Besides, the shear effect also affects the aggregate morphology. Under the shear effect, the columnar aggregates are sheared into irregularly shaped pieces. As the long axis ends of the fragments are subjected to greater shear forces relative to the short axis ends, the particles adhering to the long axis ends are stripped off and the long axis length will gradually approach the short axis. Therefore, the particle aggregates gradually tend to be spherical with the shear effect.

With the total flow unchanged and the gas-liquid two-phase flow ratio decreases from 3:1 to 1:2, the gas phase flow rate gradually becomes smaller and the liquid phase flow rate increases. As shown in Fig. 6, the number of collisions between particles becomes larger (Fig. 6b) and the Fτ and Fn imposed on the particles increase (Figs. 6c and d). However, the final stable C_d is not monotonically varying (Fig. 6a). When the two-phase flow ratio decreases from 3:1 to 2:1, as the number of collisions increases, the adhesion between particles becomes easier and

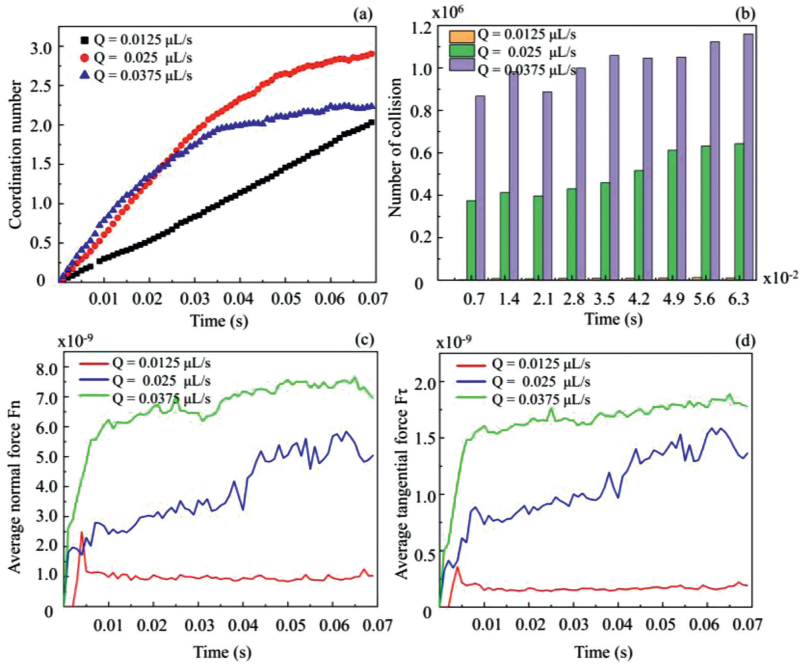

Fig. 5. Changes of the average coordination number (a), collision number (b), normal force (c) and tangential force (d) of particles at different total flow rates.

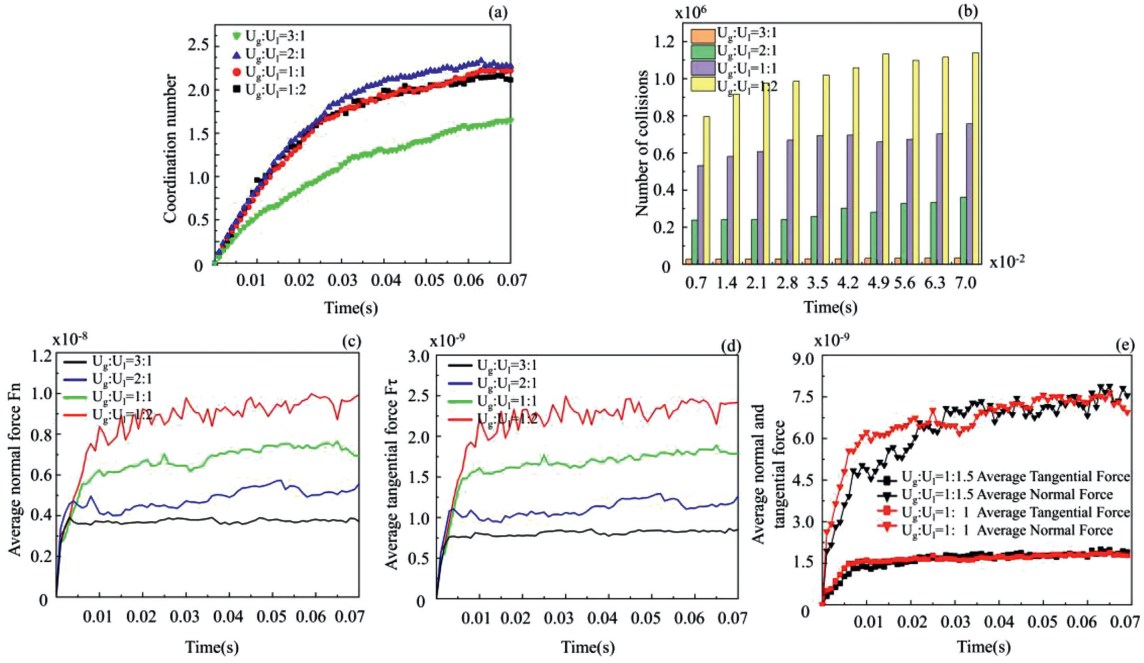

Fig. 6. Effect of gas-liquid ratio on particle morphology and coordination number: (a-d) Changes in the average coordination number, collision number, normal force, and tangential force of particles when the two-phase flow ratios are 3:1, 2:1, 1:1, and 1:2, the total flow rate is kept constant at 0.025 μL/s, and particle volume fractions of 1%. (e) Changes in the normal force when the two-phase flow ratio is changed from 1:1.5 to 1:1 and the liquid phase flow rate is kept constant at 0.0125 μL/s.

the aggregates become larger. However, when the two-phase flow ratio continues to decrease to 1:2, the aggregates become gradually smaller. Based on the above conclusions, the aggregation size is influenced by the coupling of collision frequency and shear effects. When the gas-liquid flow rate ratio is greater than or equal to 2:1, although the number of collisions is relatively small, the shear force on the aggregates is still smaller than the adhesion force between the particles, so there is no shear effect. Therefore, the aggregate size is only affected by the collision frequency at this point. Nevertheless, when the gas-liquid two-phase flow rate ratio is less than or equal to 1:1, a shear effect occurs. Although the collision number is greater than the former, it is difficult to produce adhesion between particles due to the shear effect, resulting in the reduction of aggregate size. Under the shear effect, even an increase in the number of interparticle collisions does not make the aggregates larger. Therefore, when interparticle adhesion and shear effect compete with each other, the shear effect actually dominates the effect on aggregate size.

When the gas-liquid flow ratio increases, the liquid-phase flow rate decreases, and the shear effect on the particles also decreases. Therefore, we assume that the particle shear effect is only affected by the liquid phase flow rate. To verify this assumption, a set of comparison experiments were simulated, which kept the liquid phase flow rate constant and only varied the gas phase flow rate. Fig. 6e shows the variation of $F\tau$ and Fn on the particles when the liquid phase flow rate is kept constant at 0.0125 μL/s and the gas phase flow rate is reduced from 0.01875 μL/s to 0.0125 μL/s. The results show that the magnitudes of $F\tau$ and Fn subjected to the particles basically match, which indicates that the shear effect on the particles is only related to the liquid phase flow rate. While high liquid phase flow rates produce high shear effects, they also increase the length of the slug, which leads to unequal retention time distribution. Therefore, it is necessary to optimize the gas-liquid phase flow rate ratio so that the particle aggregation size and polydispersity are reduced.

In this numerical simulation for the study of particle aggregation in gas-liquid two-phase flow, the interparticle interaction forces, interparticle adhesion, and hydrodynamics are considered. The flow field is controlled by the N-S equation, the inter-particle collision and adhesion are described based on the JKR model, and the flow field is coupled with the particle dispersion phase. The effects of particle collision number and shear effects on particle aggregation and aggregate morphology were investigated by varying the particle volume fraction, total flow rate and gas-liquid two-phase flow ratio.

As a result, when the particle volume fraction becomes larger, the number of inter-particle collisions also increases, making it easy for adhesion to occur between particles. Besides, increasing the total flow rate or decreasing the gas-liquid two-phase flow rate ratio is accompanied by increasing the collision number and shear force. The shear effect is generated when the shear force is greater than the interparticle adhesion force. Furthermore, although the particles collide with each other, inter-particle adhesion is also less likely to occur when shear effects occur, and particle aggregates stop growing.

Acknowledgments

This work was supported by the Shanghai Beyond Limits Manufacturing Project, the National Natural Science Foundation of China (Nos. 11502044, U1906233), the Fundamental Research Funds for the Central Universities (No. DUT22JC08), Dalian city supports innovation and entrepreneurship projects for high-level talents (No. 2021RD16) and Liaoning Province's Xing Liao Talents Program (No. XLYC2002108).

Supplementary materials

Supplementary material associated with this article can be found, in the online version, at doi:10.1016/j.cclet.2023.108747.

References

[1] S. Swain, P.K. Sahu, S. Beg, S.M. Babu, Curr. Drug Deliv. 13 (2016) 1290–1302.

[2] U.U.M. Nordin, N. Ahmad, N. Salim, N.S.M. Yusof, RSC Adv. 11 (2021) 29080–29101.
[3] J.Q. Wang, W.W. Mao, L.L. Lock, et al., ACS Nano 9 (2015) 7195–7206.
[4] C. Kinnear, T.L. Moore, L. Rodriguez-Lorenzo, et al., Chem. Rev. 117 (2017) 11476–11521.
[5] L. Zhang, Q. Feng, J.L. Wang, et al., ACS Nano 9 (2015) 9912–9921.
[6] L. Zhang, Q. Chen, Y. Ma, J. Sun, ACS Appl. Bio Mater. 3 (2020) 107–120.
[7] P. Stolzenburg, T. Lorenz, A. Dietzel, G. Garnweitner, Chem. Eng. Sci. 191 (2018) 500–510.
[8] G. Ochoa-Vazquez, B. Kharisov, A. Arizmendi-Morquecho, et al., IEEE Trans. Nanobiosci. 21 (2022) 135–140.
[9] D.V. Ravi Kumar, B.L.V. Prasad, A.A. Kulkarni, Chem. Eng. J. 192 (2012) 357–368.
[10] H. Huang, H. du Toit, S. Ben-Jaber, et al., React. Chem. Eng. 4 (2019) 884–890.
[11] C.H. Kwak, J.P. Park, S.S. Lee, et al., J. Nanosci. Nanotechnol. 18 (2018) 1339–1342.
[12] C.W. Wang, A. Oskooei, D. Sinton, M.G. Moffitt, Langmuir 26 (2010) 716–723.
[13] G. Schabas, C.W. Wang, A. Oskooei, et al., Langmuir 24 (2008) 10596–10603.
[14] Z. Xu, C. Lu, J. Riordon, et al., Langmuir 32 (2016) 12781–12789.
[15] V. Becker, H. Briesen, Phys. Rev. E 78 (2008) 61404–61413.
[16] V. Becker, H. Briesen, J. Colloid Interface Sci. 346 (2010) 32–36.
[17] V. Becker, E. Schlauch, M. Behr, H. Briesen, J. Colloid Interface Sci. 339 (2009) 362–372.
[18] E. De Angelis, M. Chinappi, G. Graziani, Meccanica 47 (2012) 2069–2077.
[19] A. Nikoubashman, Soft Matter 13 (2016) 222–229.
[20] C. Prohm, M. Gierlak, H. Stark, Eur. Phys. J. E 35 (2012) 80.
[21] J.F. Wilson, M. Kroupa, J. Kosek, M. Soos, Langmuir 34 (2018) 15600–15611.
[22] M. Zeidan, B.H. Xu, X. Jia, R.A. Williams, Chem. Eng. Res. Des. 85 (2007) 1645–1654.
[23] C.W. Wang, A. Bains, D. Sinton, M.G. Moffitt, Langmuir 28 (2012) 15756–15761.
[24] C.W. Wang, A. Bains, D. Sinton, M.G. Moffitt, Langmuir 29 (2013) 8385–8394.
[25] C.W. Wang, D. Sinton, M.G. Moffitt, J. Am. Chem. Soc. 133 (2011) 18853–18864.
[26] D. Qian, A. Lawal, Chem. Eng. Sci. 61 (2006) 7609–7625.
[27] P. Aussillous, D. Quere, Phys. Fluids 12 (2000) 2367–2371.
[28] W. Dijkhuizen, M.V. Annaland, J.A.M. Kuipers, Chem. Eng. Sci. 65 (2010) 1274–1287.
[29] S.B. Yeom, E.S. Ha, M.S. Kim, et al., Pharmaceutics 11 (2019) 414–465.
[30] K.L. Johnson, K. Kendall, A.D. Roberts, Proc. R. Soc. Lond. A: Math. Phys. Sci. 324 (1971) 301–313.
[31] O. Baran, A. DeGennaro, E. Rame, A. Wilkinson, AIP Conference Proceedings 1145 (2009) 409–412.
[32] Z. Peng, L. Ge, R. Moreno-Atanasio, et al., Chem. Eng. J. 396 (2020) 124738.
[33] A.A. Kulkarni, V.Sebastian Cabeza, Langmuir 33 (2017) 14315–14324.
[34] J. Subero, Z. Ning, M. Ghadiri, C. Thornton, Powder Technol. 105 (1999) 66–73.